Chinese Chemical Letters 34 (2023) 107796

Contents lists available at ScienceDirect

Chinese Chemical Letters

journal homepage: www.elsevier.com/locate/cclet

Improved multiferroic in $EuTiO_3$ films by interphase strain engineering

Yiyan Fan[a], Shiqing Q. Deng[a,b,*], Tianyu Li[a], Qinghua Zhang[c], Shuai Xu[c], Hao Li[a], Chuanrui Huo[a], Jiaou Wang[d], Lin Gu[c,g], Kuijuan Jin[c,e,f], Oswaldo Diéguez[h], Er-Jia Guo[c,e,f,**], Jun Chen[a,*]

[a] Beijing Advanced Innovation Center for Materials Genome Engineering, Department of Physical Chemistry, University of Science and Technology Beijing, Beijing 100083, China
[b] School of Mathematics and Physics, University of Science and Technology Beijing, Beijing 100083, China
[c] Beijing National Laboratory for Condensed Matter Physics and Institute of Physics, Chinese Academy of Sciences, Beijing 100190, China
[d] Institute of High Energy Physics, Chinese Academy of Sciences, Beijing 100049, China
[e] Department of Physics, University of Chinese Academy of Sciences, Beijing 100049, China
[f] Songshan Lake Materials Laboratory, Dongguan 523808, China
[g] National Center for Electron Microscopy in Beijing, School of Materials science and Engineering, Tsinghua University, Beijing 100084, China
[h] Department of Materials Science and Engineering, Faculty of Engineering, Tel Aviv University, Tel Aviv 6997801, Israel

ARTICLE INFO

Article history:
Received 26 July 2022
Revised 20 August 2022
Accepted 1 September 2022
Available online 7 September 2022

Keywords:
$EuTiO_3$
Magnetic phase transition
Polar state
Interphase strain engineering

ABSTRACT

Interphase strain engineering provides a unique methodology to significantly modify the lattice structure across a single film, enabling the emergence and manipulation of novel functionalities that are inaccessible in the context of traditional strain engineering methods. In this work, by using the interphase strain, we achieve a ferromagnetic state with enhanced Curie temperature and a room-temperature polar state in EuO secondary phase-tunned $EuTiO_3$ thin films. A combination of atomic-scale electron microscopy and synchrotron X-ray spectroscopy unravels the underlying mechanisms of the ferroelectric and ferromagnetic properties enhancement. Wherein, the EuO secondary phase is found to be able to dramatically distort the TiO_6 octahedra, which favors the non-centrosymmetric polar state, weakens antiferromagnetic Eu-Ti-Eu interactions, and enhances ferromagnetic Eu-O-Eu interactions. Our work demonstrates the feasibility and effectiveness of interphase strain engineering in simultaneously promoting ferroelectric and ferromagnetic performance, which would provide new thinking on the property regulation of numerous strongly correlated functional materials.

Perovskite oxides are of great scientific and practical interest due to their rich functional properties and strong correlations between structural degrees of freedom and order parameters [1–4]. Many works demonstrate that the intriguing physical properties, such as multiferroicity, superconductivity, magnetoresistance, and photovoltaic effects, can be effectively modulated by chemical doping, anion defects, and stain engineering [5–8]. Being a representative multiferroic candidate, perovskite $EuTiO_3$ (ETO) that exhibits a paraelectric (PE) and G-type antiferromagnetic (AFM) ground state below Néel temperature (T_N) ~5.5 K, has attracted extensive attention due to its high tunability [9]. In particular, different origins for ferroelectricity from Ti ions and magnetic moment from Eu ions ($S=7/2$) break the so-called d^0 *vs.* d^n dilemma and thus differentiate it from other systems [10]. Moreover, theoretical studies have demonstrated that by properly strain engineering ETO could transform from an antiferromagnetic (AFM)-paraelectric (PE) state to a ferromagnetic (FM)-ferroelectric (FE) state with a strong spontaneous magnetization of 7 μ_B/Eu and remnant polarization of 10 $\mu C/cm^2$ [11]. Although the importance of achieving multiferroicity in a single material for the next-generation information devices has been well recognized and the theoretically predicted properties of ETO can even rival classic ferroelectrics and ferromagnets, experimental realization of the coexistence of multi-ferroic orderings in ETO remains elusive [6,12,13].

* Corresponding authors at: Beijing Advanced Innovation Center for Materials Genome Engineering, Department of Physical Chemistry, University of Science and Technology Beijing, Beijing 100083, China.
** Corresponding author at: Beijing National Laboratory for Condensed Matter Physics and Institute of Physics, Chinese Academy of Sciences, Beijing 100190, China.
E-mail addresses: sqdeng@ustb.edu.cn (S.Q. Deng), ejguo@iphy.ac.cn (E.-J. Guo), junchen@ustb.edu.cn (J. Chen).

https://doi.org/10.1016/j.cclet.2022.107796
1001-8417/

Strain engineering, including biaxial strain, chemical strain, and interphase strain, provides an effective means to manipulate the functionalities of complex oxides [14–16]. Specifically, the biaxial substrate-film interfacial strain has been widely used in the structure and property regulation of epitaxial thin films, such as $BiFeO_3$, $LaCoO_3$, $SrTiO_3$ [17–19]. It has also been demonstrated that the interfacial strain could stabilize the ferromagnetic state below ~4 K and the ferroelectric state with a Curie temperature of ~250 K in the $EuTiO_3$-$DyScO_3$ (ETO-DSO) system [20,21]. While such ordering temperatures are still too low to meet the requirements for potential applications. Further exploration and property improvements of ETO films in the context of interfacial strain engineering have been hindered by limitations in the magnitude of mismatch-induced strain and strain relaxation along the thickness direction [22]. For the chemical strain method, generally chemical doping can not only introduce the modification of local strain states but also the inevitable changes in local electronic states, which, however, could generate unwanted impurities and properties. Moreover, the magnitude of the strain that can be introduced by chemical doping is also limited [23]. In contrast, by appropriately engineering the coherent interface between two phases, the interphase strain method can outstand in the aspects of strain magnitude and non-relaxation in the film thickness direction. For example, as large as 16.5% strain can be induced in the $PbTiO_3$/PbO system, which contributes to the significant increase in the ferroelectric remanent polarization [16]. Meanwhile, the whole regions of such interphase strain-engineered films are fully strained with a uniform strain state along the film thickness direction [24]. This, therefore, provides new opportunities for properties improvement of the ETO material. Applying interphase strain to ETO film with a large and unrelaxed strain across the film could harvest the effective regulation and considerable improvement of its properties.

In this work, by using the interphase strain method, we realize the enhanced magnetic properties and room-temperature (RT) polar states in strained ETO films engineered by a structural compatible EuO secondary phase. Atomic-scale characterizations reveal that the randomly distributed secondary phase can introduce a significant elongation in the lattice structure along the growth direction and a distortion of TiO_6 octahedra. As a result, Eu-Ti-Eu bond length, Eu-Ti-Eu bonding angle, and bandgap structure change correspondingly, evidenced by atomic imaging and spectroscopic analysis, which plays an important role in determining the enhanced ferromagnetism and room-temperature polar phase. On this basis, the underlying mechanism for the performance improvements has been clarified. By simultaneously increasing ferroelectricity and ferromagnetism of representative multiferroic candidate, ETO, using the interphase strain method, our study could be enlightening for the material design and emergent property control of not only the big multiferroic family but also for wide-ranging strongly correlated functional materials.

The EuO (EO) is chosen as the secondary phase because it can not only impose large tensile strain on ETO along the out-of-plane direction, but also prevent introducing additional impurities. The EuO has the same cubic phase as ETO with a space group of $Fm\bar{3}m$ and a larger lattice parameter of 5.142 Å than that of ETO (Fig. S1 in Supporting information). This, therefore, can ideally introduce a 24% (the compressive effect of ETO matrix on EO phase is not considered) large tensile interphase strain with a coherent ETO-EO interface. A series of thin films with different Eu contents have been fabricated on (001)-oriented STO substrates. With the increase in x (excess mole number of Eu in the target), the out-of-plane lattice parameters of the films increase (Fig. S2 in Supporting information), which suggests an effective modification of the secondary phase to the strain state of the films. The content of $x = 0.4$ is selected for thorough studies due to the largest tensile strain achieved. Since stoichiometric ratio of the target and the film would not be strictly consistent, we performed a quantitative elemental analysis of the film. As the ICP results shown in Table S1 (Supporting information), the thin film is defined as ETO-0.35EO in the following based on the actual mole ratio of Eu to Ti.

Fig. 1a shows a typical XRD θ–2θ scan of an ETO-0.35EO thin film. The distinct Laue oscillations around the (00l) deflection peaks indicate good crystalline quality and epitaxial growth of the film. The out-of-plane lattice constant of ETO-0.35EO film is determined as 4.056 ± 0.005 Å, which is significantly larger than that of bulk ETO ($a = 3.905$ Å). It is worth mentioning that although the secondary phase is introduced, the films maintain the same good crystallinity, lattice symmetry, and surface roughness as those of a single-phase ETO film (Fig. S3 in Supporting information). In addition, such films also manifest an atomically sharp substrate-film interface (Fig. S4 in Supporting information). We performed the reciprocal space mapping (RSM) near the (103) plane of the STO substrate. The result verifies that the ETO-0.35EO film is epitaxially grown on the substrate and suffers a large tensile strain of 3.7% along the c axis (Fig. 1b). Such a significant tensile strain is largely contributed by the EuO secondary phase rather than the STO-ETO mismatch strain since the in-plane lattice parameters of ETO and STO substrates are the same [21]. Note that a 1.15% (much lower than 3.7%) tensile strain in the ETO-STO system has also been reported, which should possibly come from the non-stoichiometry induced chemical strain [20]. The atomic-scale structural analysis was performed using spherical aberration-corrected scanning transmission electron microscopy (STEM). It can be seen from the low-mag images that the secondary phase EO is randomly distributed within the ETO matrix, as marked by the dashed region in Fig. 1c. No evident impurities other than the EO phase are found.

To investigate the details of the local structure between the two phases, atomic resolution cross-sectional high-angle annular dark-field STEM (HAADF-STEM) images along the [100] zone axis of the ETO-0.35EO film are acquired and shown in Fig. 1d. Since the atomic intensity is approximatively proportional to $Z^{1.7}$ for HAADF-STEM images, brighter and darker contrast correspond to heavier (Eu, $Z = 63$) and lighter (Ti, $Z = 22$) atoms, respectively. It can be noted that the contrast of the STEM image divides it into two regions. Wherein, the yellow shaded region is the EO secondary phase at the [110] zone axis and the other region is the ETO phase at the [100] zone axis, which both are consistent with the structure model (Figs. S1c and d). Noteworthily, these two phases characterize a coherent interface. As shown in the schematic model in Fig. 1e, the ETO (100) plane can match well with EO (110) plane along the in-plane direction. The a value of EO (3.64 Å, equal to $a_{(110)}/2$) is close to a_{ETO} and a_{STO}, which benefits the epitaxial growth of heterogeneous films. A local enlargement of the ETO-EO interface STEM image verifies the match fashion of the two phases (Fig. 1f). The corresponding intensity profile across the interface manifests a clear intensity drop from the left side to the right, double confirming the ETO (right)-EO (left) two phases structure (Fig. 1g). Therefore, the STEM analysis proves that the coexistence and perfect match of the two phases plays a dominant role in the generation of large external tensile strain.

Intriguing structural modifications with large tensile strain could lead to emergent physical properties. As shown in Fig. 2a, the temperature-dependent magnetization (M-T curve) of ETO-0.35EO thin film was obtained at the magnetic field of 1 kOe applied along the in-plane direction. It suggests the emergence of an FM state in the thin film with Curie temperature at T_c ~7.2 K. Inset shows the field-dependent magnetization (M-H curve) of ETO-0.35EO thin film at 2 K. Well-defined magnetic hysteresis loop with a finite coercive field of ~100 Oe provides unambiguous evidence on the ferromagnetism in the films at low temperatures. As the applied magnetic field increases to 5 T, M approaches ~ 6.5 μ_B/Eu, which is close to the theoretical value of 7 μ_B/Eu [27]. More im-

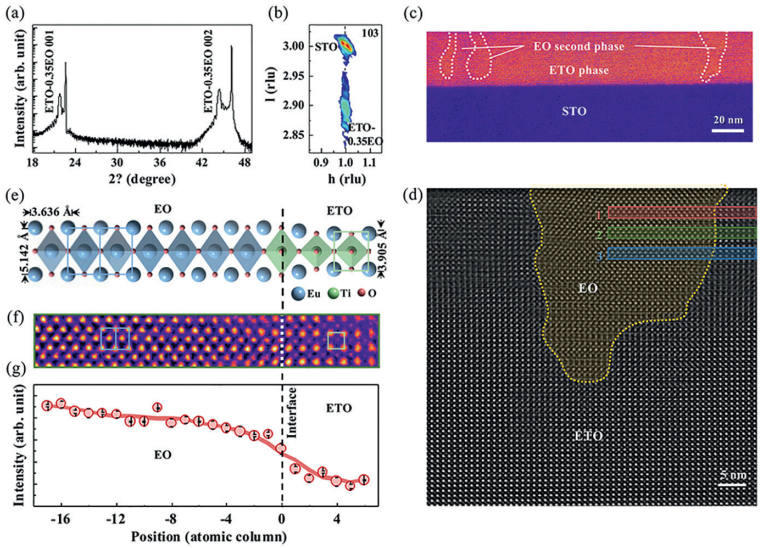

Fig. 1. Structural characterizations of ETO-0.35EO thin film. (a) XRD $\theta-2\theta$ scan of an ETO-0.35EO film. (b) RSM around the (103) plane of the substrate. (c) Low-magnified cross-sectional STEM image of an ETO-0.35EO film grown on STO substrate. Dashed white circles mark the EO second phase region. (d) High-magnified HAADF-STEM image of representative interphase between ETO and EO. Boundaries between the two phases are indicated by yellow dashed lines. (e) Schematic and (f) STEM image of an atomic-scale interphase structure. (g) Averaged intensity profile extracted from regions 1 to 3 in (d). Error bars are the standard deviation.

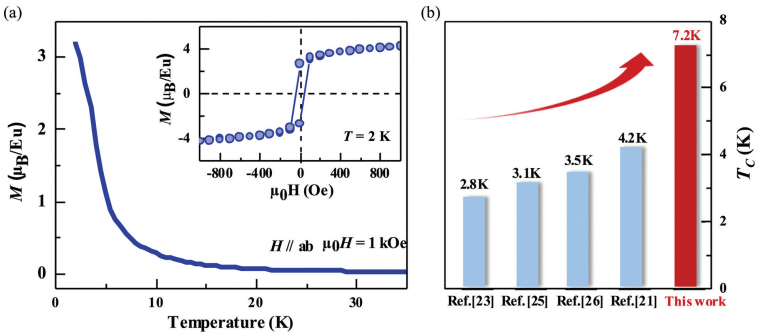

Fig. 2. Enhanced ferromagnetic properties in ETO-0.35EO thin film. (a) *M-T* curve of an ETO-0.35EO film. Measurements were performed under a magnetic field of $\mu_0 H$ =1 kOe along the in-plane direction after field cooling. Inset shows the *M-H* hysteresis loop at 2 K. (b) Comparison of T_C of ETO-0.35EO film with previous studies [21,23,25,26]. The magnetic transition temperature of interphase strain-engineered ETO films is increased by 70%.

portantly, it is evidenced that the ETO-0.35EO epitaxial film modulated by interphase strain exhibits the highest Curie temperature of 7.2 K. Such a T_c enhances by 70% compared to the highest value previously reported in single-phase ETO thin films (Fig. 2b) [21,23,25,26].

The large elongation along the out-of-plane direction generally induces a significant increase in the *c/a* ratio within films, which would provide the polar structure [16]. Optical second harmonic generation (SHG) investigations were conducted in ETO-0.35EO film to check this possibility (see experimental details in Supporting information). The inset of Fig. 3a shows the schematic configuration of the SHG setup. The temperature-dependent SHG intensity of ETO-0.35EO thin film is shown in Fig. 3a, where a kink at 180 K indicates that the sample undergoes a phase transition. Such a phase transition is also confirmed by frequency-dependent dielectric spectra shown in Fig. 3b. We note that the SHG intensity is nonzero in the whole temperature range between 80 and 300 K, which could imply that the polar structure in ETO-0.35EO thin film may still retain at RT. This polar state can result from asymmetric phases with polarity in ETO-0.35EO thin film since the interface between the two phases distorts the surrounding lattice to lower symmetry and gives rise to large local polarization at the nanoscale [28]. To eliminate the possible influence from the substrate, we measured the SHG signals from the pure STO substrate and the film separately (Fig. S5 in Supporting information). The SHG intensity of ETO-0.35EO film is an order of magnitude larger than that of STO substrate, suggesting a negligible role of STO substrate.

Figs. 3c–f show the SHG polar figures of ETO-0.35EO film recorded at different temperatures. Figs. 3c and e, d and f are the $I_{p\text{-}out}$ and $I_{s\text{-}out}$ signals as a function of polarization angle when a polarized light incident on the ETO-0.35EO film at 100 and 300 K, respectively. The experimental data can be fitted with the *m* and *P4mm* point groups at 100 and 300 K, respectively. These results demonstrate that the ETO-0.35EO film is still a polar structure with a different point group than that of bulk ETO ($Pm\bar{3}m$) [29]. Hence, the spontaneous polarization at RT may occur in the ETO-0.35EO thin film, which is superior to the reported strained ETO films with a ferroelectric transition temperature of 250 K [21]. The SHG signal is normally generated in materials lacking inversion symmetry, it is a necessary but insufficient condition for the ferroelectricity [30,31]. Therefore, we measured the electrical hysteresis loop of ETO-0.35EO film at 100 K as well (Fig. S7 in Supporting Information). Unfortunately, the measurement of the hysteresis loop at RT cannot be performed perfectly to provide valuable information due to the large leakage current. We hypothesize that its intrinsic ferroelectricity is submerged in the leaky backbone, which could be related to the semi-conductivity and small bandgap (1.12 ev) of the EuO phase [32].

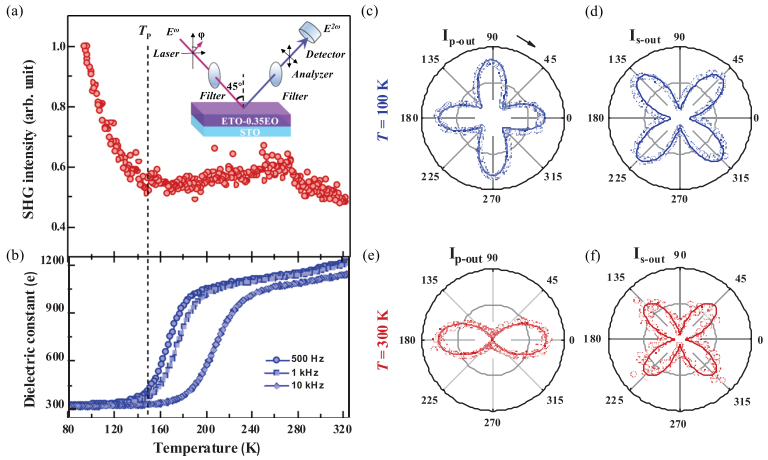

Fig. 3. Polar state in ETO-0.35EO thin film confirmed by SHG and dielectric spectra. Temperature-dependent (a) SHG intensity and (b) dielectric spectra of an ETO-0.35EO film. Inset shows the schematic diagram of the SHG setup carried out in the reflective mode. The p- and s-polarized lights were incident on the films with an angle of 45° with respect to the incident plane. $I_{p\text{-}out}$ and $I_{s\text{-}out}$ signals were collected as a function of polarized angle (φ) at (c, d) 100 K and (e, f) 300 K, respectively. Open circles and solid lines represent the experimental data and theoretical fits, respectively. Dielectric spectra were measured at different frequencies (f = 500 Hz, 1 kHz, and 10 kHz).

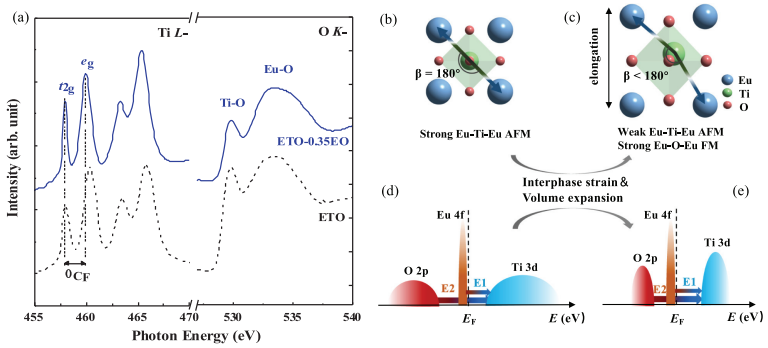

Fig. 4. Manipulation of electronic state in ETO-0.35EO thin film by interphase strain. (a) XAS at Ti *L*- and O *K*-edges in an ETO-0.35EO film. The dashed lines show the reference spectra for Ti^{4+} [37] and O *K*-edges in the stoichiometric ETO films. Schematic diagram of dominant magnetic interactions in (b) unstrained ETO films and (c) interphase-strained ETO films. Corresponding electronic band structures of (d) unstrained and (e) interphase-strained ETO films. E_1 represents the band gap between the Eu and Ti orbitals whereas the E_2 represents the band gap between Ti and O orbitals.

To illustrate the intrinsic effects of interphase strain on the electronic states [33,34], X-ray absorption spectroscopy (XAS) was conducted at RT. As shown in Fig. 4a, the typical features at Ti *L*-edges confirm the valence state of Ti ions in the ETO-0.35EO film is +4, indicating that the ETO and EO phases are stoichiometric with negligible charge transfer and minor oxygen vacancies. According to crystal field theory, in an ideal TiO_6 octahedral, the five degenerate 3d-orbitals of Ti atoms split into triply degenerate low-energy t_{2g} orbitals and doubly degenerate high-energy e_g orbitals, where the difference between the t_{2g} and e_g orbitals represents the crystal field splitting energy (Δ_{CF}) [35]. It is noted that the distance between Ti 3d t_{2g} and Ti 3d e_g orbitals in ETO-0.35EO film is significantly smaller than those in the standard Ti^{4+} (black line at left), revealing that Δ_{CF} has further decreased because of the distorted TiO_6 octahedron [36,37]. As displayed in XAS of O-K edges, the intensity of the Eu-O peak in ETO-0.35EO film is higher than that in a single-phase ETO film. These results suggest that the existence of the EO phase in the film, that is, Eu excess in our designed ceramic target transfers to the films as an EO secondary phase. The XAS results are consistent with the STEM and ICP measurements (Table S1 in Supporting information).

Previous works demonstrated that there should co-exist three key magnetic interactions in bulk ETO [38]: (1) AFM interactions between the nearest-neighbor Eu ion pairs along the [001] direction; (2) FM interactions between the second nearest-neighbor Eu ion pairs along the [101] direction (indirect exchange *via* O 2p states); (3) AFM interactions between the third nearest-neighbor Eu ion pairs along the [111] direction (super exchange *via* Ti 3d states). DFT calculations by Akamatsu *et al.* [39] show that the main origin of AFM state in bulk ETO is the super exchange interactions between Eu-Ti-Eu along the [111] direction. It strongly depends on the bond length and bond angle of Eu-Ti-Eu. Upon imposing the interphase strain in ETO-0.35EO thin film, the out-of-plane lattice of ETO stretches and simultaneously Ti atoms move upwards, which can result in a corresponding change in the bond length of Eu-Ti-Eu. Meanwhile, the average Eu-Ti-Eu bond angles of ETO unit cells with different distances away from the interface reduce from 180° to around 170° ± 5°, as evidenced by the quantitative analysis of the atomic STEM image (Fig. S6 in Supporting information). Figs. 4b and c illustrate schematics of unstrained cubic ETO and strained ETO along the [001] direction, respectively. The change of Eu-Ti-Eu bond lengths and angles along the [111] direction in the ETO region is a direct consequence of the strong stretching effect by the secondary EO phase. The dramatic structural modification affects the AFM interactions that dominate their magnetic states, supported by the Goodenough-Kanamori-Anderson rule [40–42].

In addition, the energy band and electron distribution are determined by strain as well. The qualitative relationship between spin state and lattice distortion has been reported previously [43–46]. Shin *et al.* have summarized in both theoretical and experimental manners the change of band gap between Eu 4f, Ti 3d and O 2p orbitals with increasing volume of unit cell. The schematics atomic orbitals in strained-free and strained ETO are present in Figs. 4d

and e, respectively [47–49]. In the strained ETO with a reduced Eu-Ti-Eu bond angle, the band gap between Ti 3d and O 2p (E_2) reduces while the band gap between Eu 4f and Ti 3d (E_1) increases. As a result, the fully occupied O 2p orbitals migrate easily to Ti 3d orbitals. The electronic transfer in this manner will benefit the enhancement of the ferromagnetic interactions between the second nearest-neighbor Eu ion pairs (*via* changed O 2p orbitals).

In summary, a ferromagnetic state with enhanced Curie temperature emerged in the interphase strain-engineered ETO thin films. The introduced secondary EO phase leads to a significant elongation along the out-of-plane direction. The dramatic distortion of TiO_6 octahedra effectively affects the Eu-Ti-Eu bond length and bonding angle, which are directly linked to their electronic configurations. Eventually, the AFM interactions between the third nearest Eu ion pair (*via* Ti^{4+}) are weakened whereas the FM interactions between the second nearest Eu ion pairs (*via* O^{2+}) are enhanced, which favors the ferromagnetic state over the antiferromagnetic state. Additionally, the polar state is achieved at RT in ETO-0.35EO film as well, providing the possibility to acquire a single-phase multiferroic materials and magnetoelectric coupling through strain optimization by the interphase strain method. This study demonstrates that effective interphase strain tuning using structural compatible phases is readily applied to other strongly correlated materials and clearly exhibits its unique advantages for improving functionalities over other means.

Declaration of competing interest

The authors declare that they have no known competing financial interests or personal relationships that could have appeared to influence the work reported in this paper.

Acknowledgments

This work was supported by the National Key Basic Research Program of China (Nos. 2020YFA0309100 and 2019YFA0308500), the National Natural Science Foundation of China (Nos. 21825102, 22001014, 11294029, 11974390, 11721404), the China National Postdoctoral Program for Innovative Talents (No. BX20200043), China Postdoctoral Science Foundation (No. 2021M690366), the Beijing Nova Program of Science and Technology (No. Z191100001119112), the Beijing Natural Science Foundation (No. 2202060), the Guangdong-Hong Kong-Macao Joint Laboratory for Neutron Scattering Science and Technology, the Strategic Priority Research Program (B) of the Chinese Academy of Sciences (No. XDB33030200), the Fundamental Research Funds for the Central Universities, China (Nos. 06500145 and FRF-IDRY-20–039), and State Key Laboratory of New Ceramic and Fine Processing Tsinghua University (No. KF202110). This work made use of the resources of the Beijing National Center for Electron Microscopy at Tsinghua University.

Supplementary materials

Supplementary material associated with this article can be found, in the online version, at doi:10.1016/j.cclet.2022.107796.

References

[1] J.P. Locquet, J. Perret, J. Fompeyrine, et al., Nature 394 (1998) 453–456.
[2] R.V Helmolt, J. Wecker, B. Holzapfel, et al., Phys. Rev. Lett. 71 (1993) 2331–2333.
[3] J. Wang, J.B. Neaton, H. Zheng, et al., Science 299 (2003) 1719–1722.
[4] A.R. Damodaran, E. Breckenfeld, Z. Chen, et al., Adv. Mater. 26 (2014) 6341–6347.
[5] D. Kan, V. Anbusathaiah, I. Takeuchi, Adv. Mater. 23 (2011) 1765–1769.
[6] D.G. Schlom, L.Q. Chen, C.J. Fennie, et al., MRS Bull. 39 (2014) 118–130.
[7] S.V. Kalinin, N.A. Spaldin, Science 341 (2013) 858–859.
[8] T.R. McGuire, M.W. Shafer, R.J. Joenk, H.A. Alperin, S.J. Pickart, J. Appl. Phys. 37 (1966) 981–982.
[9] C.L. Chien, S. DeBenedetti, Phys. Rev. B 10 (1974) 3913–3922.
[10] N.A. Hill, J. Phys. Chem. B 104 (2000) 6694–6709.
[11] C.J. Fennie, K.M. Rabe, Phys. Rev. Lett. 97 (2006) 267602.
[12] J. Ma, J. Hu, Z. Li, C.W. Nan, Adv. Mater. 23 (2011) 1062–1087.
[13] N.A. Spaldin, R. Ramesh, Nat. Mater. 18 (2019) 203–212.
[14] D. Kan, L. Pálová, V. Anbusathaiah, et al., Adv. Funct. Mater. 20 (2010) 1108–1115.
[15] K.J. Choi, M. Biegalski, Y.L. Li, et al., Science 306 (2004) 1005–1009.
[16] L.X. Zhang, J. Chen, L.L. Fan, et al., Science 361 (2018) 494–497.
[17] Z. Chen, X. Zou, W. Ren, et al., Phys. Rev. B 86 (2012) 235125.
[18] E.J. Guo, R.D. Desautels, D. Keavney, et al., Phys. Rev. Mater. 3 (2019) 014407.
[19] J.H. Haeni, P. Irvin, W. Chang, et al., Nature 430 (2004) 758–761.
[20] K. Tanaka, K. Fujita, Y. Maruyama, et al., MRS Proc. 1454 (2012) 149–159.
[21] J.H. Lee, L. Fang, E. Vlahos, et al., Nature 466 (2010) 954–958.
[22] A.R. Chaudhuri, M. Arredondo, A. Hähnel, et al., Phys. Rev. B 84 (2011) 054112.
[23] W. Li, R. Zhao, L. Wang, et al., Sci. Rep. 3 (2013) 2618.
[24] T.Y. Li, S.Q. Deng, H. Liu, et al., Adv. Mater. 33 (2021) e2008316.
[25] Y. Lin, E.M. Choi, P. Lu, et al., ACS Appl. Mater. Interfaces 12 (2020) 8513–8521.
[26] K. Fujita, N. Wakasugi, S. Murai, et al., Appl. Phys. Lett. 94 (2009) 062512.
[27] V. Goian, S. Kamba, O. Pacherová, et al., Phys. Rev. B 86 (2012) 054112.
[28] H.J. Liu, H.J. Wu, K.P. Ong, et al., Science 369 (2020) 292.
[29] A. Bussmann-Holder, J. Köhler, R.K. Kremer, J.M. Law, Phys. Rev. B 83 (2011) 212102.
[30] Y.R. Shen, Annu. Rev. Phys. Chem. 40 (1989) 327–350.
[31] M. Trassin, G.D. Luca, S. Manz, M. Fiebig, Adv. Mater. 27 (2015) 4871–4876.
[32] N.J.C. Ingle, I.S. Elfimov, Phys. Rev. B 77 (2008) 121202.
[33] M. Allieta, M. Scavini, L.J. Spalek, et al., Phys. Rev. B 85 (2012) 184107.
[34] H. Akamatsu, Y. Kumagai, F. Oba, K. Fujita, K. Tanaka, et al., Adv. Funct. Mater. 23 (2013) 1864–1872.
[35] S. Morpurgo, J. Chem. Educ. 84 (2007) 151–155.
[36] A.J. Millis, Phys. Rev. B 53 (1996) 8434–8441.
[37] Y. Cao, X. Liu, M. Kareev, et al., Nat. Commun. 7 (2016) 10418.
[38] P.W. Anderson, Phys. Rev. 79 (1950) 350–356.
[39] H. Akamatsu, Y. Kumagai, F. Oba, et al., Phys. Rev. B 83 (2011) 214421.
[40] J.B. Goodenough, Phys. Rev. 100 (1955) 564–573.
[41] J. KanamorI, J. Phys. Chem. Solids 10 (1959) 87–98.
[42] P.W. Anders, Solid State Phys 14 (1963) 99–214.
[43] T. Kasuya, IBM J. Res. Dev. 14 (1970) 214–223.
[44] R. Ranjan, H. Sadat Nabi, R. Pentcheva, J. Phys. Condens. Matter 19 (2007) 406217.
[45] R. Ranjan, H.S. Nabi, R. Pentcheva, J. Appl. Phys. 105 (2009) 053905.
[46] J.B. Goodenou, Book Rev. 458 (1963) 1273.
[47] D. Shin, I. Kim, S. Song, et al., J. Am. Ceram. Soc. 104 (2021) 4606–4613.
[48] J.H. Lee, X. Ke, N.J. Podraza, et al., Appl. Phys. Let. 94 (2009) 202509.
[49] X.Y. Wang, S.Q. Zhen, Y. Min, et al., J. Appl. Phys. 122 (2017) 194102.